J Forensic Sci, January 2007, Vol. 52, No. 1
doi:10.1111/j.1556-4029.2006.00327.x
Available online at: www.blackwell-synergy.com

Cédric Neumann,[1] *M.Sc.; Christophe Champod,*[2] *Ph.D.; Roberto Puch-Solis,*[1] *Ph.D.; Nicole Egli,*[2] *M.Sc.; Alexandre Anthonioz,*[2] *M.Sc.; and Andie Bromage-Griffiths,*[1] *B.Sc.*

Computation of Likelihood Ratios in Fingerprint Identification for Configurations of Any Number of Minutiæ

ABSTRACT: Recent court challenges have highlighted the need for statistical research on fingerprint identification. This paper proposes a model for computing likelihood ratios (LRs) to assess the evidential value of comparisons with any number of minutiæ. The model considers minutiae type, direction and relative spatial relationships. It expands on previous work on three minutiae by adopting a spatial modeling using radial triangulation and a probabilistic distortion model for assessing the numerator of the LR. The model has been tested on a sample of 686 ulnar loops and 204 arches. Features vectors used for statistical analysis have been obtained following a preprocessing step based on Gabor filtering and image processing to extract minutiae data. The metric used to assess similarity between two feature vectors is based on an Euclidean distance measure. Tippett plots and rates of misleading evidence have been used as performance indicators of the model. The model has shown encouraging behavior with low rates of misleading evidence and a LR power of the model increasing significantly with the number of minutiæ. The LRs that it provides are highly indicative of identity of source on a significant proportion of cases, even when considering configurations with few minutiæ. In contrast with previous research, the model, in addition to minutia type and direction, incorporates spatial relationships of minutiæ without introducing probabilistic independence assumptions. The model also accounts for finger distortion.

KEYWORDS: forensic science, fingermark, fingerprint, identification, individualization, likelihood ratio, statistics

Recent challenges of fingerprint evidence in court have strengthened the need for statistical research to underpin the fingerprint identification process. Indeed in its decision in United States v Byron Mitchell (1), the court highlighted that "the actual standard employed by any given FBI examiner falls somewhere between these extremes, yet the FBI's reliance on an unspecified, subjective, sliding-scale mix of "quantity and quality of detail" makes meaningful testing elusive, for it is difficult to design an experiment to test a hypothesis with unspecified parameters." Our view is that a systematic acquisition of statistical data describing fingerprint selectivity through adequate modeling will help to address fundamental issues raised in the area of fingerprint identification. Our purpose is to offer latent fingerprint examiners with models allowing the assessment of the strength of evidence in a robust and reliable manner.

This paper proposes a model, which assesses statistically the strength of the comparison between latent marks and suspect prints. The model can provide support for comparisons with more than three corresponding minutiae. This research work is an extension of previous work devoted to three minutiæ only (2). Our purpose is not to demonstrate the individuality of a complete and well-reproduced fingerprint, but to assess the evidential contribution of fingermarks that can be partial, distorted and with a poor signal/noise ratio.

Adopting a likelihood ratio (LR) framework is essential to weigh together both the variability on fingerprints originating from the same finger due to skin elasticity and the variability on fingerprints originating from different fingers. The general LR model has been described elsewhere (3). The computation of a LR calls for the estimation of two probability density functions. The probability density function in the numerator of the LR is an estimation of the variability of the features when left at several occasions by the same donor (within finger variability). The probability density function in the denominator is an estimation of the variability of the features when they come from different fingers (between fingers variability). To relate the concept of LR with traditional fingerprint identification practice, it is useful to view the exclusion as a LR of zero (the numerator of the LR being zero). Individualization is reached when the LR is infinite (the denominator of the LR being zero). Dealing with cases between these two extremes is the purpose of this statistical analysis.

This paper describes the image preprocessing and feature extractions, which were used to acquire fingerprint data and minutiae information. In addition to minutia type and direction, the model captures the spatial relationship between minutiæ by using a radial triangulation. The organization and the exploitation of these data using a LR are then presented. Finally, the performance of this multiminutia system on selected datasets is illustrated. Tippett plots (4–6) are used for assessing the accuracy of this LR-based system. Tippett plots provide a graphical representation of the general magnitude of the LRs obtained from our method under the two considered hypothesis of common source and of different sources. They also provide the discriminative power of the system and the rates of potentially misleading evidence of the system.

Preprocessing

Images acquired to investigate the numerator and denominator of the LRs have been fully or partly processed according to the

[1]The Forensic Science Service, Trident Court, 2920 Solihull Parkway, Birmingham Business Park, Birmingham B37 7YN, U.K.
[2]Ecole des Sciences Criminelles, Institut de Police Scientifique, Batochime, Quartier Sorge Université de Lausanne, CH-1015 Lausanne-Dorigny, Switzerland.

Received 6 Feb. 2006; and in revised form 26 July 2006; accepted 1 Sept. 2006; published 10 Dec. 2006.

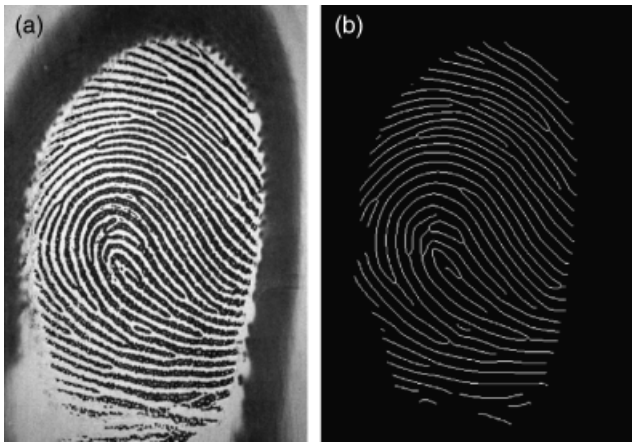

FIG. 1—*(a) Original gray scale image, (b) cleaned skeleton obtained from (a).*

methodology previously described (2). The images were treated using Gabor filtering (7,8) and skeletonized after a manual check (and manual correction if needed by trained operators) of the accuracy of the binary representation with respect to the initial grayscale image. An example is shown in Fig. 1.

After having cleaned and healed the skeleton of the remaining noise, we obtained clean skeletons for both the within and the between variability images. Features of statistical interest are extracted from them.

Spatial Modeling Using Radial Triangulation

The spatial arrangement of minutiæ is modeled through a triangulation of a polygon whose vertices are minutia locations. Once the polygon is constructed a number of triangulations can be used. A fingermark from a crime-scene does not usually exhibit information on its location within a fingerprint, and in particular, its orientation within the print. The construction of the polygon therefore requires the definition of a unique ordering of the minutia locations. Hence allowing for the structure of the triangulated polygon to be rotation invariant; in other words, the polygon should be encoded in a structure that does not change irrespective of which minutia we start coding. This concept will be revisited later in this section once radial triangulation is introduced as it plays an important role in the calculation of the denominator of the LR.

Let us assume that we have a method for defining a unique polygon for a given set of minutia locations. Many methods provide a triangulation of a polygon, including Delaunay triangulations and its constrained versions. Delaunay triangulation had been used in our earlier work on three minutiæ (2). However, the triangulation of polygons representing spatial arrangement of minutiae, using these methods, does not provide a triangulation that is robust to fingerprint distortion. Furthermore, such triangulated polygons cannot be captured in a structure that is invariant depending on the starting minutiæ: we would require either precomputing a large number of triangulations depending on the starting minutia or computing these triangulations when computing a LR. Obviously, the number of triangulations will increase significantly faster than the number of minutiae and therefore, there will clearly be issues with the amount of computer storage and processing time required.

In this paper we propose a method that we called "radial triangulation" (9) for the construction of a polygon and its triangulation that gives a structure that is rotation invariant and more

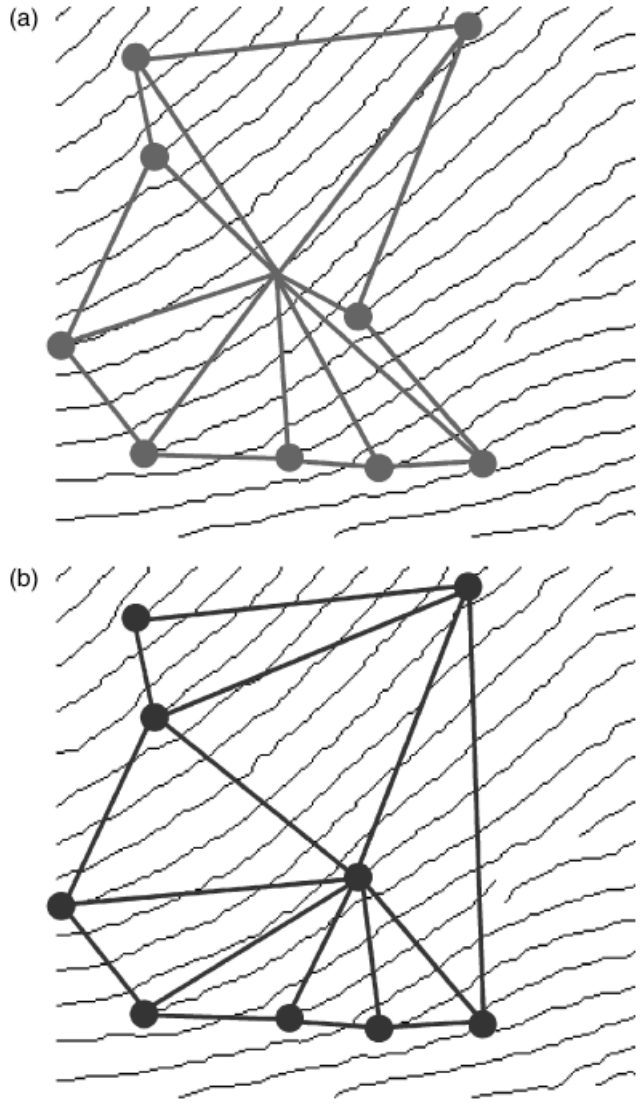

FIG. 2—*(a) The radial triangulation of a set of nine minutiæ, (b) the Delaunay triangulation of the same set of minutiæ.*

robust to fingerprint distortion, and which does not require a large amount of storage space and computing time. Given a set of minutia locations there is a unique centroid defined by the arithmetic mean of the coordinates. The centroid is then used for ordering the minutia locations in a "radar" manner, which is used to define a unique polygon. Given this polygon the centroid is also used for triangulating it: radii are added from the vertices of the polygon to the centroid. Figure 2*a* presents the polygon and radial triangulation of a set of 12 minutiæ while Fig. 2*b* shows the standard Delaunay triangulation for the same configuration of minutiæ. Any vertex in the radial triangulation is linked to two other vertices and to the centroid, while in the Delaunay triangulation the number of connections for each vertex can vary.

Feature Vector Extraction

The evidential assessment of a comparison of a finger mark from the crime scene, subsequently referred as the mark, and a suspect's fingerprint, subsequently called the print, requires the comparison of features from the mark and the print. The radial triangulation gives a platform for extracting these features and records them as a list number called a feature vector. The general

form of the feature vector for a configuration of N minutiæ is,

$$[GP, \{T_1, RA_1, R_1, L_{1,2}, S_1\}, \{T_2, RA_2, R_2, L_{2,3}, S_2\}, \ldots, \{T_N, RA_N, R_N, L_{N,1}, S_N\}] \quad (1)$$

where GP is the general pattern of the fingerprint, T_k is the type of minutia k (k takes value from 1 to N), RA_k is the direction of minutia k relatively to the image, R_k is the radius of minutia k to the centroid, $L_{k,k+1}$ is the length of the polygon side between minutia k and minutia $k+1$, S_k is the area of the triangle defined by minutiæ k, $k+1$, and the centroid.

The radial triangulation introduced earlier allows for feature vectors with a small number of entries: the number of sets in curly brackets is the same as the number of minutiæ in the configuration. In contrast, a feature vector based on the Delaunay triangulation used previously (2) would require the addition of a large number of extra diagonals, which would make the sets in the curly brackets very large. This additional information would need a much larger storage space and would imply larger computational cost.

The feature vector of a minutia configuration from a print is denoted by x, while the feature vector of a configuration from a mark is denoted by y. The entries for the vectors are identified with subscripts x and y, respectively. We therefore have,

$$x = [GP_x, \{T_{x,1}, RA_{x,1}, R_{x,1}, L_{x,1,2}, S_{x,1}\}, \{T_{x,2}, RA_{x,2}, R_{x,2}, L_{x,2,3}, S_{x,2}\}, \ldots, \{T_{x,N}, RA_{x,N}, R_{x,N}, L_{x,N,1}, S_{x,N}\}] \quad (2)$$

$$y = [GP_y, \{T_{y,1}, RA_{y,1}, R_{y,1}, L_{y,1,2}, S_{y,1}\}, \{T_{y,2}, RA_{y,2}, R_{y,2}, L_{y,2,3}, S_{y,2}\}, \ldots, \{T_{y,N}, RA_{y,N}, R_{y,N}, L_{y,N,1}, S_{y,N}\}]$$

We can rearrange the feature vector to separate the information on the configuration provided by the general pattern from the specific information on each minutia as $x = [GP_x, x_s]$ where

$$x_s = [\{T_{x,1}, RA_{x,1}, R_{x,1}, L_{x,1,2}, S_{x,1}\}, \{T_{x,2}, RA_{x,2}, R_{x,2}, L_{x,2,3}, S_{x,2}\}, \ldots, \{T_{x,N}, RA_{x,N}, R_{x,N}, L_{x,N,1}, S_{x,N}\}] \quad (3)$$

Similarly we can write a feature vector from the mark as $y = [GP_y, y_s]$.

LRs for Configurations of N Minutiæ

In this section, we describe a LR specifically designed for assessing the evidential value of the link between a print and a mark (10). Formally, we can write:

$$LR = \frac{p(x, y|S, I)}{p(x, y|\bar{S}, I)} = \frac{p(GP_x, GP_y, x_s, y_s|S, I)}{p(GP_x, GP_y, x_s, y_s|\bar{S}, I)}$$

where S sets the hypothesis that a considered suspect left the mark at the crime scene. More particularly, that a particular minutiae configuration from a define finger from this suspect corresponds to a particular minutiae configuration on the mark. $\bar{S}$ sets the hypothesis that somebody else left the mark at the crime scene; I encapsulates any other information that may be relevant to the case.

The previous equation can be expanded as

$$LR = \underbrace{\frac{p(x_s, y_s|GP_x, GP_y, S, I)}{p(x_s, y_s|GP_x, GP_y, \bar{S}, I)}}_{LR_{s|g}} \times \underbrace{\frac{p(GP_x, GP_y|S, I)}{p(GP_x, GP_y|\bar{S}, I)}}_{LR_g} = LR_{s|g} \times LR_g \quad (4)$$

The overall LR is then a multiplication of two components. The second, LR_g, is associated with the information on the general pattern while the first $LR_{s|g}$, weighs the contribution of the specific information on a minutia configuration given the information on the general pattern.

The numerator of LR_g is 1. Indeed, by assuming that the mark and the print configurations are both from the considered suspect and correspond, there are no doubts that the general pattern information in the respective feature vectors should be the same. The value of the denominator of this LR can only be related to the characteristics of the mark as it is assumed that the considered suspect is not involved. Hence, this value is the probability that a feature vector originates from a fingerprints having general pattern GP_y. This probability can be computed using the occurrence of general patterns based on values compiled from the National Crime Information Center (11). Table 1 gives the percentages for most general patterns.

The $LR_{s|g}$ in Eq. (4) is computed using the formula,

$$LR_{s|g} = \frac{p(d(x_s, y_s)|GP_x, GP_y, S, I)}{p(d(x_s, y_s)|GP_x, GP_y, \bar{S}, I)} \quad (5)$$

where $d(x_s,y_s)$ is a distance between two configurations of minutiæ encoded in feature vectors x_s and y_s [Eq. (3)].

Given an N-minutia polygon, the structure of its feature vector y_s is driven by the choice of the starting minutia during the feature extraction process. This dependence is made explicit by adding an extra subscript indicating the minutia first listed in the feature vector. Therefore, there are N possible ways to record the same feature vector, more specifically,

$$\begin{aligned}
y_{s,1} &= [\{T_{y,1}, RA_{y,1}, R_{y,1}, L_{y,1,2}, S_{y,1}\}, \{T_{y,2}, RA_{y,2}, R_{y,2}, L_{y,2,3}, S_{y,2}\}, \ldots, \{T_{y,N}, RA_{y,N}, R_{y,N}, L_{y,N,1}, S_{y,N}\}] \\
y_{s,2} &= [\{T_{y,2}, RA_{y,2}, R_{y,2}, L_{y,2,3}, S_{y,2}\}, \{T_{y,3}, RA_{y,3}, R_{y,3}, L_{y,3,4}, S_{y,3}\}, \ldots, \{T_{y,1}, RA_{y,1}, R_{y,1}, L_{y,1,2}, S_{y,1}\}] \\
&\vdots \\
y_{s,N} &= [\{T_{y,N}, RA_{y,N}, R_{y,N}, L_{y,N,1}, S_{y,N}\}, \{T_{y,1}, RA_{y,1}, R_{y,1}, L_{y,1,2}, S_{y,1}\}, \ldots, \{T_{y,N-1}, RA_{y,N-1}, R_{y,N-1}, L_{y,N-1,N}, S_{y,N-1}\}]
\end{aligned}$$

Distance $d(x_s,y_s)$ is therefore defined as

$$d(x_s, y_s) = \min\{d(x_s, y_{s,i}) : i = 1, 2, \ldots, N\} \quad (6)$$

The calculation of this distance is very efficient because the structure of the feature vectors is invariant to fingerprint rotations and

TABLE 1—*Percentages of general patterns used to compute LR_g.*

General Pattern	Percentages (%)
Arches	9
Whorls	24
Left loops	33
Right loops	34

there is no need for extracting extra information when computing each of the $d(x_{s,}y_{s,i})$. This property is given by the radial triangulation presented earlier.

The calculation of each of the $d(x_s,y_{s,i})$ is computed in two steps. First the entries of the feature vectors are normalized so that they take a similar range of values, and second, an Euclidean distance is computed. The normalization is done with respect to the values of the entries of the feature vectors in the reference database, and it guarantees that the contribution of each entry is not confounded with the units of measurement.

The probability density functions for both the numerator and the denominator of the LR can now be computed. For the numerator, the distance $d(x_s,y_s)$ is an instance of distances between feature vectors that originated from the same finger because it is conditioned on S being true. The calculation of many such distances is used for estimating the probability density function for the numerator. We therefore refer to the variability of these distances as within-finger variability. For the denominator $d(x_s,y_s)$ is an instance of a distance between a mark feature vector and a noncorresponding feature vector because of the conditioning on $\bar{S}$ being true. Many distances between the mark feature vector and feature vectors extracted from a reference population are used for estimating the probability density function for the denominator. The variability in these distances is thus called between finger variability. These two densities have been estimated using mixtures of normal distributions, using the EM convergence algorithm (12). Mixtures of three normal distributions have been used to estimate within-finger probability density functions and mixtures of four normal distributions have been used to estimate the between-finger ones. The area under the mixtures of normal distributions are normalized to 1 for both the numerator and the denominator of the LR. Both densities are estimated for the computation of the LR of each particular mark. Details on the acquisition of the relevant databases for estimating both density functions are given in the next section.

Data Acquisition

We will separately describe data informing the within finger variability for the numerator of the LR from data informing the between variability for the denominator of the LR.

Within Finger Variability

For the estimation of the within finger variability of configurations of three minutiæ, a database of 216 fingerprint images was constituted from 54 applications under different distortion conditions of four fingers from two people (two fingers each) (2). As expected, it appears that under distortion, some minutiae of a given finger are present on all images, while others are only present on part of the dataset. Although it is possible to estimate the effect of distortion on configurations of a small number of minutiae based on this dataset, it would be more difficult to extract a sufficient set of configurations with a larger number of minutiae to study the distortion phenomena. It was realized that such a procedure would be unsuitable for a model intended to deal with configurations of N minutiæ and, therefore, a distortion model was built for obtaining virtually distorted minutia configurations from a given configuration without the need of further sampling. For the sake of clarity of explanation this distortion model is presented for triangles, but it can be deployed for any polygon.

Distortion Model Description—Distortion in a fingerprint can both increase and decrease distances between features when the skin is either stretched or compacted. This affects the location of all features and therefore a reference point for comparing distorted distances needs to be chosen. The centroid was chosen as a reference point for consistency with the design of the feature vector. For a given triangle, distortion alters distances between the centroid and vertices. This model proposes that these distances can be independently decreased or increased due to distortion. Figure 3 shows a schematic representation of the model for a triangle. The solid-line triangle represents a triangle obtained from a suspect's fingerprint where the vertices are minutia features. The brackets surrounding each vertex represent the range of values that the radii can take due to distortion. The dotted-line triangle shows a triangle obtained from the solid-line triangle using radial distortion.

The same modeling ideas can be applied to minutia direction by representing it with a line segment starting from each vertex where the segment has the same angle as the minutia for this vertex. The end-point coordinate can then be distorted using radial distortion as described above and shown in Fig. 3. Given a triangle extracted from a fingerprint of a suspect, the radial distortion model is fully specified by stating the standard deviations for each of the radii, that is, three radii for the vertices and three radii for the directions. The triangle from the suspect is specified by its vertex coordinates from the original image and the minutia directions also with respect the original image. The dependence on the coordinate system of the original image will be later removed by computing distances between triangles.

Distortion Model Estimation—The distortion model for a triangle requires six standard deviations to be specified, three for distances between vertices and three for distances to the line segments that represent minutia direction. Data collected on distorted triangles from the middle finger (ulnar loop) of the volunteer with the highest distorted fingerprints have been used to estimate these parameters. This database contains 75 sets of triangles. One of the sets of triangles is displayed in Fig. 4*a*.

For each triangle set, the radius of each vertex and each direction segment was computed. The mean value μ and the standard deviation σ for this set were computed. Therefore for each set of triangles we computed three mean values and three standard deviations for vertex radii and the same number for direction. Figure 5 displays a plot of the mean and standard deviations for vertex radii. In this plot we can see that standard deviation has the tendency to increase as a function of mean value, and that the standard deviation vary for each mean. The variability can be explained by the variability on the number of triangles in each set. The

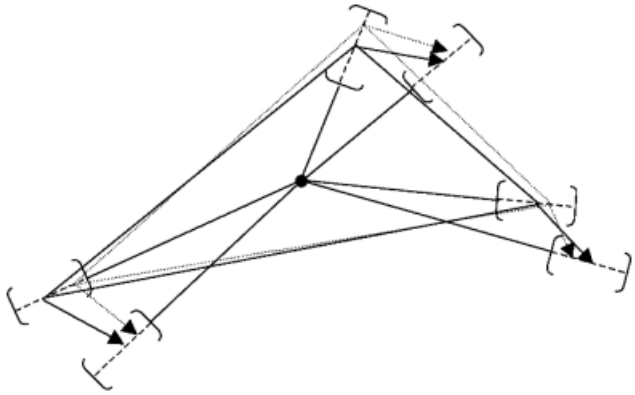

FIG. 3—*Distortion model description. The solid-line represents a minutiæ configuration extracted from a fingerprint and the dotted triangle is a minutiæ configuration distorted triangle.*

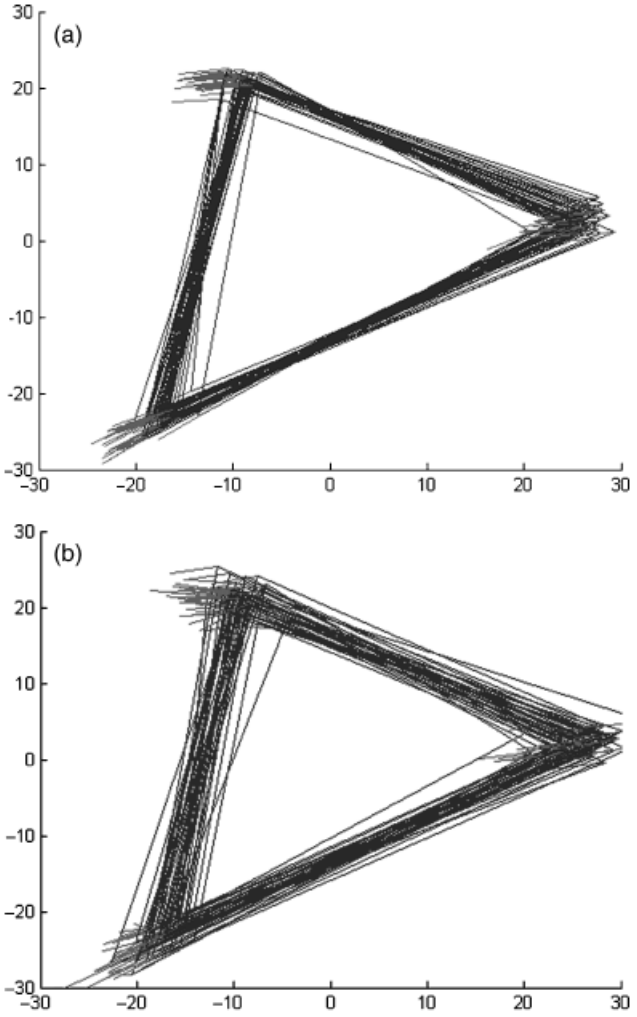

FIG. 4—*(a) Triangles extracted from distortion data, (b) triangles generated using the distortion modeling.*

increment of the standard deviation along with the mean values is modeled by a regression line estimated from the data. The estimated regression line is $\mu = 0.9+0.02\sigma$, drawn as the solid line that pass through the data. However, this line is biased by lower standard deviation due to low number of triangles in some sets.

This bias can be removed by shifting the regression line upwards through setting the intercept to 2.5, that is, $\mu = 2.5+0.02\sigma$. This shifted regression line is also plotted with a solid line on Fig. 5. Notice that the shift is quite large but it does not have a large influence to the LR because it is the denominator that dominates relatively the magnitude of the resulting LR.

Figure 4*b* displays triangles generated with the radial distortion model corresponding to the triangles extracted from distorted print displayed in Fig. 4*a*. Notice that, as expected, our model gives more variability in the triangles size and shape and minutia direction.

Between Finger Variability

Four datasets are available for the investigation of the between finger variability (Table 2). The two first datasets (ulnar loops) have been acquired during previous study (13), the remaining datasets (arches) have been acquired during this research effort. At this stage, we decided to keep separate the datasets in order to investigate the effect of a change of general pattern and finger number on the LRs. All datasets of fingerprints originate from a population of randomly selected males that had been registered within the Swiss criminal justice fingerprint database. The minutiæ locations, types, and directions were extracted from all the images for all datasets.

As for the study on three minutiæ configurations (2), reference databases of configurations were built from these fingerprint images in order to study the variability between these configurations. Although the model has the capacity to deal with configurations of any number of minutiæ, this study was limited to its behavior with configurations of three to 12 minutiæ. Therefore, reference databases for configurations from three to 12 minutiæ were built by sampling configurations into the fingerprint images.

Ten thousand configurations have been sampled for each different combination of finger number/general patterns and for each number of minutiæ in the configurations. The sampling method for a reference database of configurations of N minutiæ is as follows:

- A fingerprint image within the desired finger number/general dataset is randomly selected.
- A minutia on this fingerprint image is randomly selected.
- The $N-1$ closest minutiæ (in terms of Cartesian distances) are selected and the feature vector is extracted following the procedure described previously.
- The extracted minutia configurations are compared against the already extracted configurations to ensure that a configuration is not selected more than once.

Results

Our aim is to assess the behavior of the model to gain a better understanding of its performance. Moreover, its performance can be different for fingerprints exhibiting different general patterns. Two general patterns have been investigated: ulnar loops and arches; furthermore, the behavior of the model has been studied when different finger numbers and different hands are considered.

The performances of the model have been assessed using Tippett plots, which were constructed with the results of 1000 $LR_{s|g}$ computed for comparisons where the print and the mark originating from the same source and 1000 $LR_{s|g}$ for comparisons of prints and marks originating from different sources. LR_g has not been taken into account at that point. Indeed, with respect to Eq. (4), it would only have produced an upward shift of the results toward larger LRs.

To compute $LR_{s|g}$ in Eq. (5) for same-source comparisons, the print configuration is obtained by randomly selecting, without replacement, a configuration from the reference database. A set of 101 distorted configurations is then generated from this print configuration using the distortion model previously described. One of the generated configurations is selected as the mark and the remaining 100 are used to compute the within-distribution probability density function for the numerator of the LRs. The probability density function for the denominator is estimated from the reference database.

To compute $LR_{s|g}$ in Eq. (5) for different-source comparisons, the print configuration is chosen by randomly selecting, without replacement, a configuration from the reference database. A second configuration is randomly selected without replacement and is used as the mark. This configuration is selected such as it does not come from the same person as the first one. A set of 100 distorted configurations for the estimation of the within variability is then generated from the print configuration using the distortion

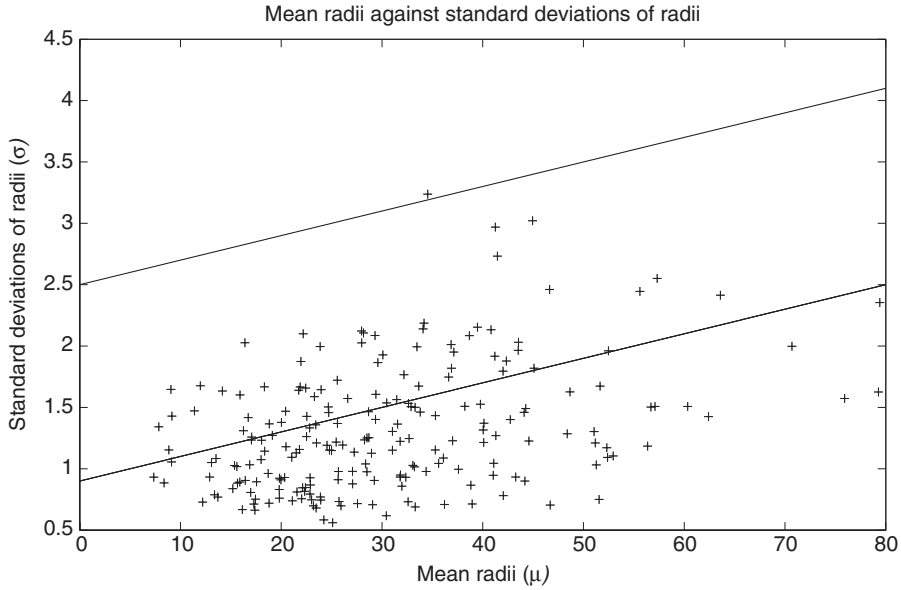

FIG. 5—*Mean distances against standard deviations of the distances.*

model previously described. This set is used to compute the within-distribution probability density function for the numerator of the LRs. The density function for the denominator is estimated from the reference database.

The choice for a resampling procedure of 1000 LRs has been made to ensure reproducibility of the Tippett plots obtained.

A Tippett plot is a specific representation of the distribution of LRs obtained for test cases of same source comparisons (S is true) and different source comparisons ($\bar{S}$ is true). On the x-axis, the $\log 10(LR_{s|g})$ is given. On the y-axis, one minus the cumulative probability distribution of the LRs is given. The Tippett plot gives then one minus the cumulative distribution for respectively the LRs computed for same-source comparisons (called LR true on the Tippett plot—dash line) and the LRs computed for different source comparisons (called LR false on the Tippett plot—solid line). These plots provide a graphical representation of the magnitude increment of the LRs along with the number of minutiae in configurations. These plots allow also a study of the accuracy of the model by comparing the proportions of misleading evidence. We have defined two rates of misleading results as follows (2):

RMED: rate of misleading evidence in favor of the defense. The percentage of all $LR_{s|g}$ computed knowing the prosecution proposition S is true that are below or equal to 1. On the Tippett plots, this rate is denoted LR true ≤ 1.

RMEP: rate of misleading evidence in favor of the prosecution. The percentage of all $LR_{s|g}$ computed knowing defense proposition $\bar{S}$ is true that are above or equal to 1. On the Tippett plots, this rate is denoted LR false ≥ 1.

TABLE 2—*Distribution of general patterns in the set of fingerprints used to assess between finger variability.*

Description	Number
Ulnar loops from right fore fingers	321
Ulnar loops from right middle fingers	365
Arch from right fore fingers	73
Arch from left fore fingers	131

It is important to emphasize that the rates of misleading evidence can be defined differently (e.g., for casework) by shifting its definition threshold (here fixed at a LR of 1). For example, it is possible to reduce the amount of RMEP, and hence favor the suspect, by increasing the value of the threshold (to 10 or 100). RMEP and RMED being linked, such an increase will result, for the model, in an increase of the rejection rate of comparisons that are truly from the same source, but will reduce the rate of reporting misleading evidence when the mark and the print truly originate from different sources.

Behavior of the Proposed Model for Configurations of Three to Twelve Minutiæ on Different General Patterns and Finger Numbers

Owing to the low number of samples in the reference population database, it was likely that some configurations would appear

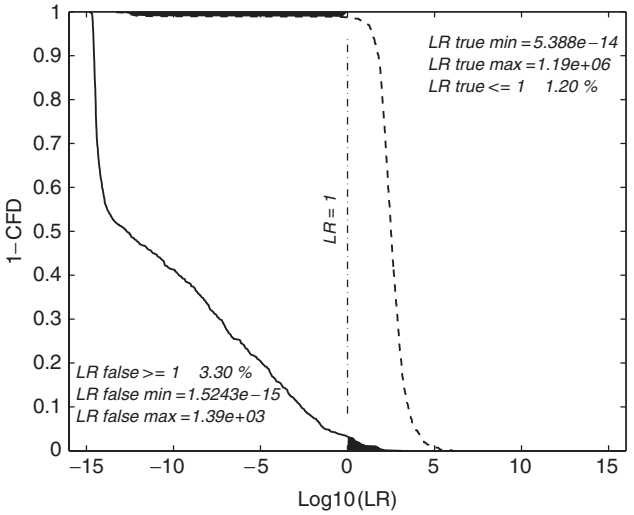

FIG. 6—*Tippett plots for configurations of three minutiæ on right middle fingers of ulnar loops (likelihood ratio [LR] false, solid line; LR true, dash line).*

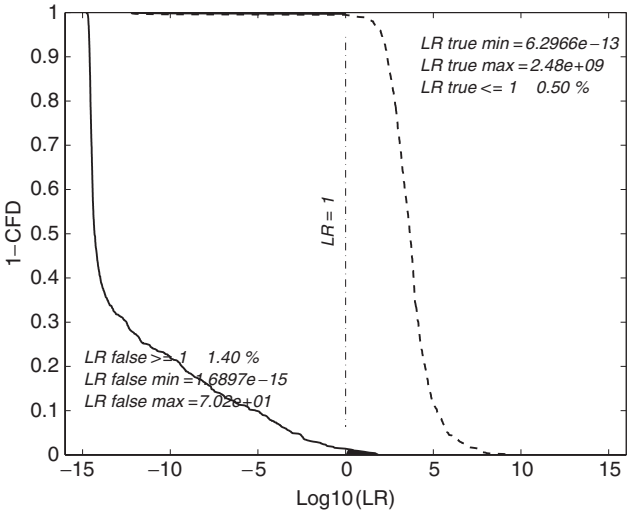

FIG. 7—*Tippett plots for configurations of four minutiæ on right middle fingers of ulnar loops (likelihood ratio [LR] false, solid line; LR true, dash line).*

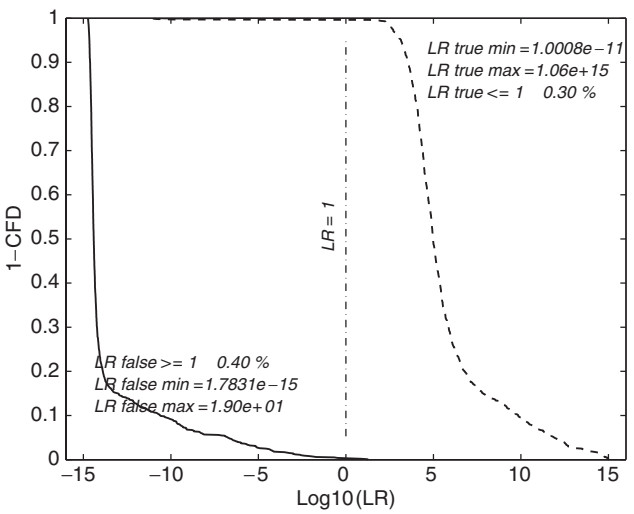

FIG. 9—*Tippett plots for configurations of six minutiæ on right middle fingers of ulnar loops (likelihood ratio [LR] false, solid line; LR true, dash line).*

extremely specific, and therefore, that resulting LRs might have meaningless values. Thus, we have chosen to limit the model by setting a threshold of 10^{-15} for the minimum density that either the numerator or the denominator of the LR is allowed to take. This is a default value aiming at stressing the limits of statistical estimation when reaching very small densities. It should be emphasized that the robustness of this default value has not been fully investigated and would require further work. In other words, LR of 10^{15} reflects extremely strong evidence but should be taken with an element of caution in terms of accuracy.

The evolution of LRs for the different patterns when the number of minutiæ increases from three to twelve minutiæ has been studied using reference databases sampled from the datasets as described previously. An example of the evolution of the Tippett plots is given for ulnar loops on the right middle finger in Figs. 6–15.

We have summarized the results obtained for the computation of the LRs true for all the combinations considered of general pattern/finger number below (Figs. 16–19) by reporting the percentage of LRs smaller than 10,000, between 10,000 and a billion (1000 million) and above a billion. The RMEP and RMED for each Tippett plot are also reported in Table 3.

As expected, the discriminating power of the model increases significantly with the number of minutiæ. Note that the threshold of 10^{-15} for the denominator prevents the LR from being greater than 10^{15}. It is interesting to observe the similar behavior of the model on the two considered general patterns as well as on arch general pattern on both hands. It is also worth noticing the significant fraction of LRs, which are below a billion, even for configurations of 12 minutiæ. When considering the RMEP and RMED of the system, the small magnitude of these rates demonstrates the accuracy of the system.

Discussion and Conclusion

The results show that the approach adopted here is robust, the magnitude of LRs obtained under both propositions (S and $\bar{S}$)

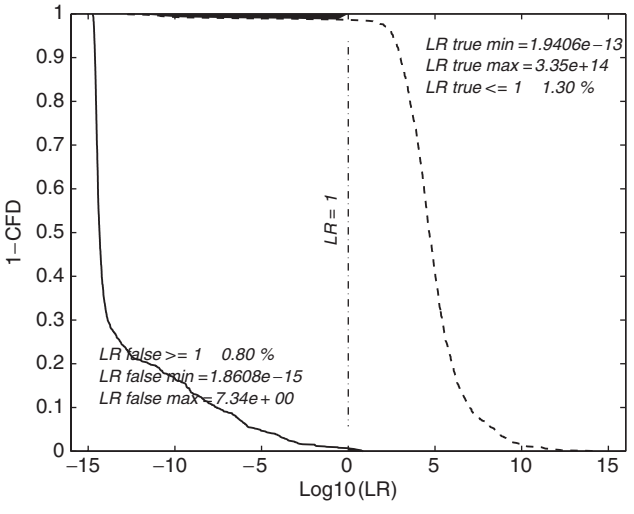

FIG. 8—*Tippett plots for configurations of five minutiæ on right middle fingers of ulnar loops (likelihood ratio [LR] false, solid line; LR true, dash line).*

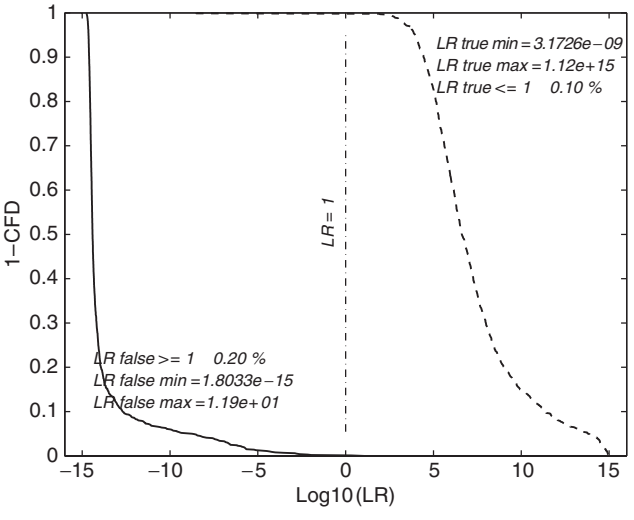

FIG. 10—*Tippett plots for configurations of seven minutiæ on right middle fingers of ulnar loops (likelihood ratio [LR] false, solid line; LR true, dash line).*

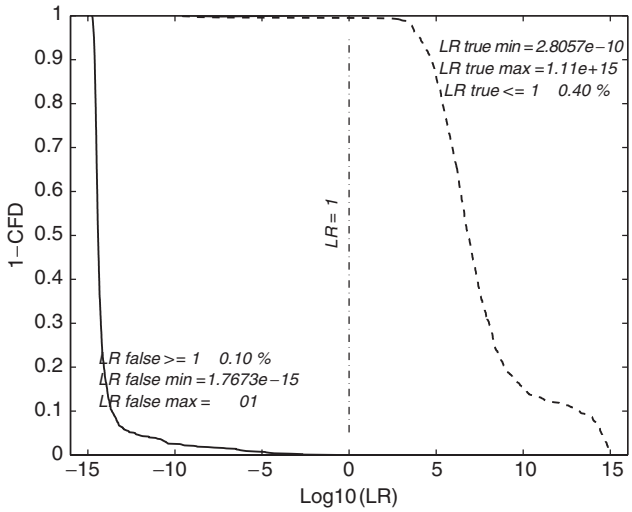

FIG. 11—*Tippett plots for configurations of eight minutiæ on right middle fingers of ulnar loops (likelihood ratio [LR] false, solid line; LR true, dash line).*

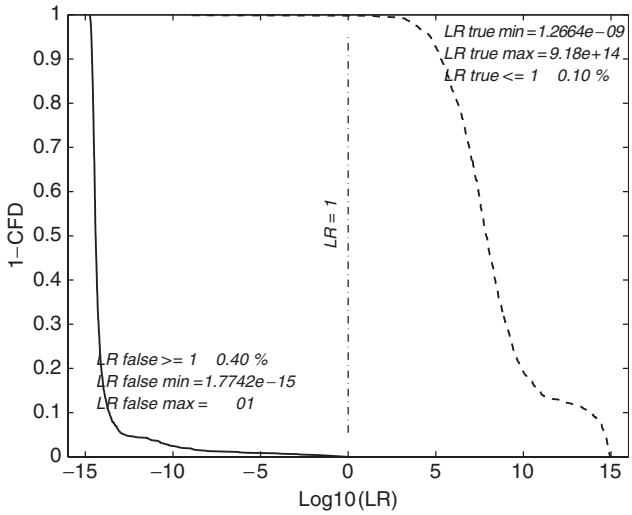

FIG. 12—*Tippett plots for configurations of nine minutiæ on right middle fingers of ulnar loops (likelihood ratio [LR] false, solid line; LR true, dash line).*

stresses the major evidential contribution small portions of fingermark (from three minutiæ) can provide. The Tippett plots computed for the different general patterns and for the different fingers on both hands show similar behaviors.

When the number of minutiæ is increased, the system has a very promising discriminating power and the LRs that it provides are very indicative of the true state under both the prosecution and the defense hypotheses. The model is able to support very strongly or strongly either hypothesis on a significant proportion of cases, even when considering configurations with few minutiæ. It has low rates of misleading evidence for both the prosecution and the defense hypotheses. The RMEP is slightly higher that the corresponding one in favor of the defense, especially for configurations of few minutiæ. This may led to the argument that the model favors the prosecution. This issue may have to be considered before any operational use. The increase of the RMEP, which can be observed for configurations of eight to twelve minutiæ on fingers with arch general patterns, can be explained by a sampling effect due to the small size of the available datasets. Indeed due to the

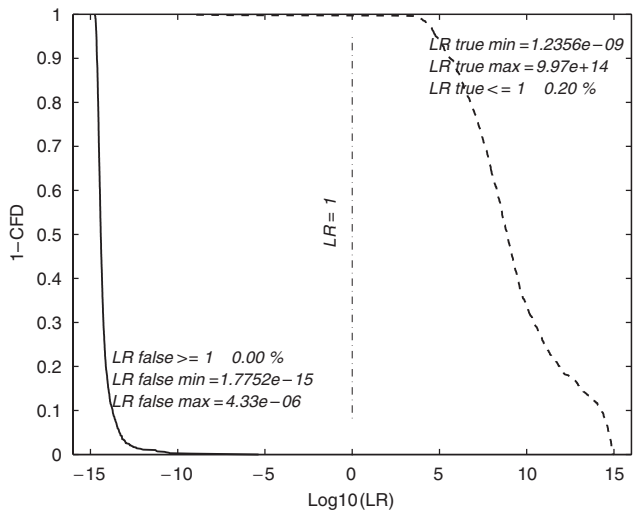

FIG. 13—*Tippett plots for configurations of 10 minutiæ on right middle fingers of ulnar loops (likelihood ratio [LR] false, solid line; LR true, dash line).*

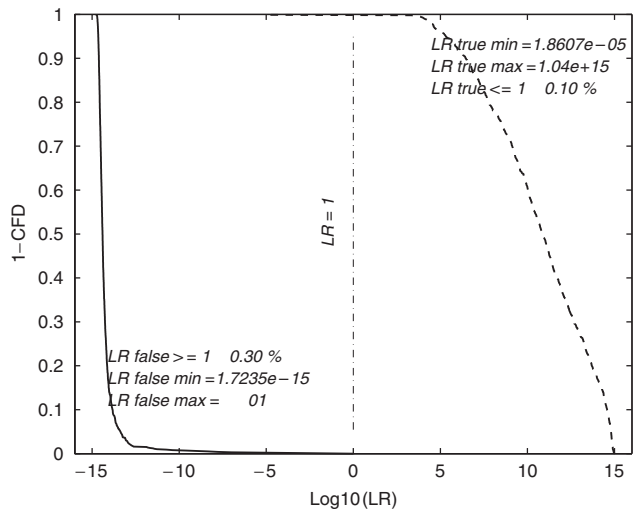

FIG. 14—*Tippett plots for configurations of 11 minutiæ on right middle fingers of ulnar loops (likelihood ratio [LR] false, solid line; LR true, dash line).*

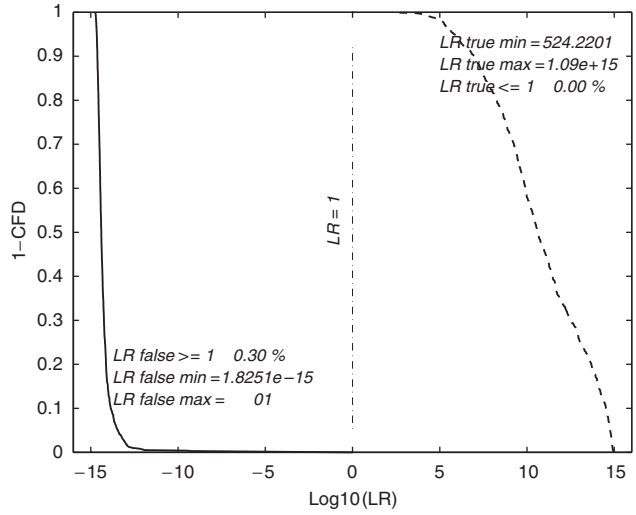

FIG. 15—*Tippett plots for configurations of 12 minutiæ on right middle fingers of ulnar loops (likelihood ratio [LR] false, solid line; LR true, dash line).*

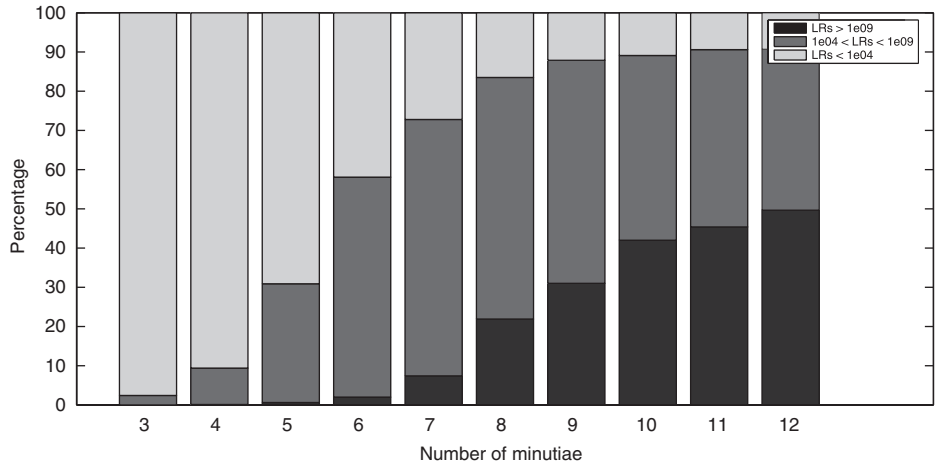

FIG. 16—*Evolution of the LRs for arch general patterns on right fore fingers.*

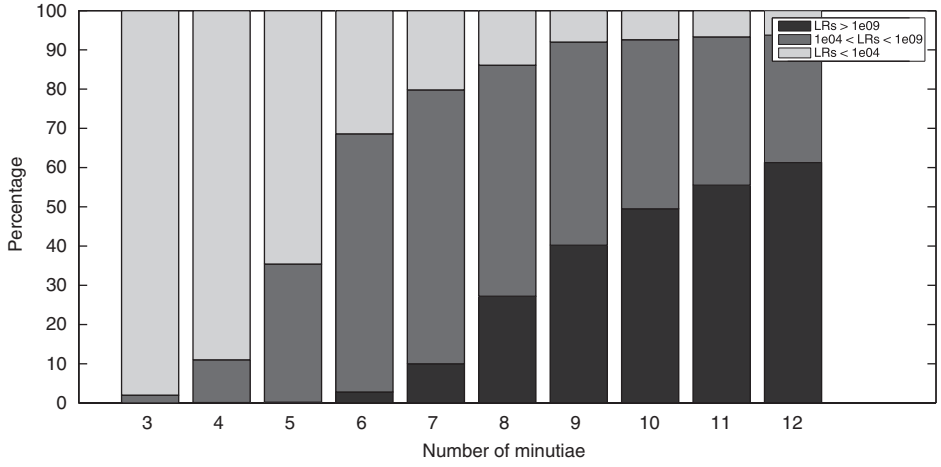

FIG. 17—*Evolution of the LRs for arch general patterns on left fore fingers.*

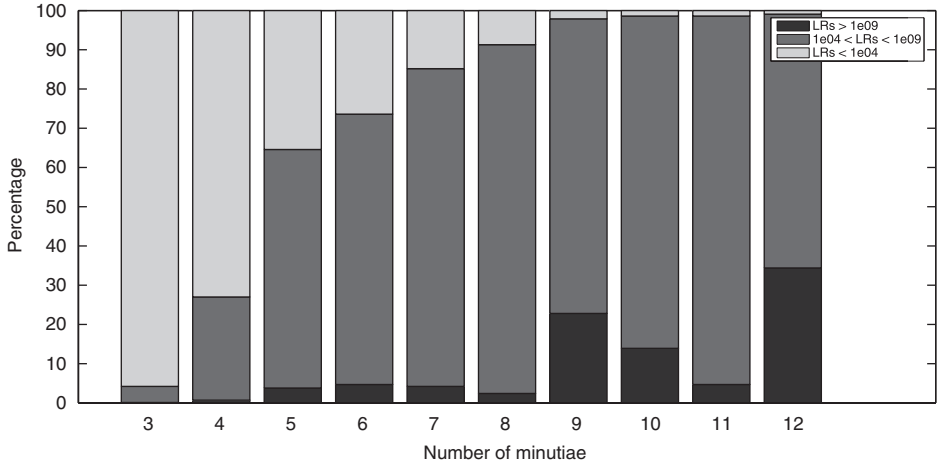

FIG. 18—*Evolution of the LRs for ulnar general patterns on right fore fingers.*

limited size of the database, the task of finding close (in terms of the distance we defined) configurations from a random source is more and more difficult as the number of minutiae increases.

We observed differences in the LRs obtained as a function of the general pattern. The interpretation of this observation is difficult at this stage. Indeed to compute the numerator of the LR, a distortion model has been proposed and validated on a series of 54 ulnar loops. This model has been applied regardless of the finger number or general pattern. The model used for the numerator is then a proxy that allows assignment of what we believe is a

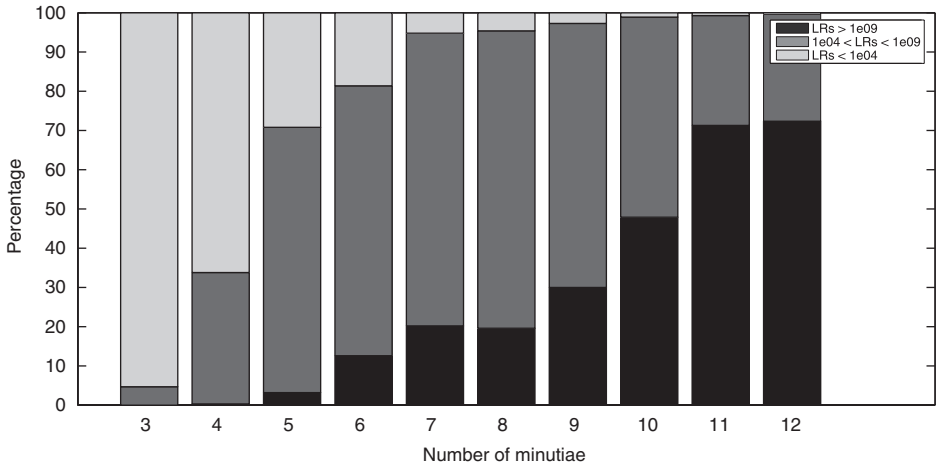

FIG. 19—*Evolution of the LRs for ulnar general patterns on right middle fingers.*

TABLE 3—*Rate of misleading evidence in favor of the prosecution (RMEP) and in favor of the defense (RMED) for ulnar loops and arches on fingers from right and left hands for configurations of three to twelve minutiæ.*

	Arch				Ulnar Loop			
	Right Fore Finger		Left Fore Finger		Right Fore Finger		Right Middle Finger	
	RMEP (%)	RMED (%)	RMEP (%)	RMED (%)	RMEP (%)	RMED (%)	RMEP (%)	RMED (%)
3 minutiæ	4.90	1.10	3.50	0.40	3.00	0.40	3.30	1.20
4 minutiæ	1.60	0.50	1.10	0.30	1.40	0.30	1.40	0.50
5 minutiæ	0.60	0.60	0.90	1.10	0.90	0.50	0.80	1.30
6 minutiæ	0.50	0.60	0.70	0.80	0.10	0.30	0.40	0.30
7 minutiæ	0.40	0.70	0.00	0.80	0.00	0.40	0.20	0.10
8 minutiæ	1.20	0.20	0.50	0.10	0.30	0.20	0.10	0.40
9 minutiæ	1.10	0.20	1.00	0.40	0.10	0.10	0.40	0.10
10 minutiæ	2.80	0.00	0.90	0.20	0.10	0.10	0.00	0.20
11 minutiæ	2.60	0.20	2.10	0.10	0.20	0.10	0.30	0.10
12 minutiæ	1.80	0.00	3.90	0.10	0.10	0.10	0.30	0.00

Note that the 0 in the table means that there were no observations for 1000 simulations.

reasonable numerator of the LR. Another explanation of the observed differences between the different general patterns and fingers might be a sampling effect due to the small size of the datasets. Further research is required to assess whether the effect of general pattern and finger number is real.

It is fair to say that the above results constitute only the first step toward the validation of the reliability and robustness of the model. However, the model developed fulfils most of the gaps identified following the establishment of the state of the art (14): it captures spatial relationships between minutiæ; it takes into account their types; it models the within-finger variability due to distortion; it is based on data and reduces to a minimum the number of underlying distributional and independence assumptions. Finally, computation can be undertaken conditioning on finger number and general pattern. These results have been achieved using a basic "Euclidean" type distance measure between feature vectors. No doubt additional research on the metric itself could lead to even more discriminative and probative results.

Whatever the metric used, it is advised that this effort be pursued and that work toward a more complete validation plan of the model before any operational use. However, these results demonstrate that developing an objective method to assess partial fingerprint is fully achievable from a three-minutia problem as we reported earlier (2) up to a multiminutia environment.

Acknowledgment

The research is supported by the U.S. Technical Support Working Group contract DAAD05-03-C-0038.

References

1. United States v Byron Mitchell: Court of Appeals for the Third Circuit. No 02-2858 (April 29, 2004).
2. Neumann C, Champod C, Puch-Solis R, Egli N, Anthonioz A, Meuwly D. Computation of likelihood ratios in fingerprint identification for configurations of three minutiæ. J Forensic Sci 2006;51(6):1255–66.
3. Aitken CGG, Taroni F. Statistics and the evaluation of evidence for forensic scientists. 2nd ed. Chichester: John Wiley & Sons Ltd., 2004.
4. Evett IW, Buckleton JS. Statistical analysis of STR data. In: Carraredo A, Brickmann B, Bär W, editors. Advances in forensic hæmogenetics. Heidelberg: Springer-Verlag, 1996:79–86.
5. Meuwly D. Reconnaissance de locuteurs en sciences forensiques: L'apport d'une approche automatique. Ph.D. Thesis. Université de Lausanne, Institut de Police Scientifique et de Criminologie, Lausanne, Switzerland, 2001.
6. Drygajlo A, Meuwly D, Alexander A. Statistical and bayesian interpretation of evidence in forensic automatic speaker recognition. Proceeding of the 8th European Conference on Speech Communication and Technology (Eurospeech—Interspeech 2003); 2003 September 1–4, The International Speech Communication Association, Geneva, Switzerland, 2003;689–92.

7. Hong L, Wan Y, Jain A. Fingerprint image enhancement: algorithm and performance evaluation. IEEE Trans Pattern Anal Mach Intell 1998;20:777–89.
8. Thai R. Fingerprint image enhancement and minutiae extraction. Dissertation.The University of Western Australia, School of Computer Science and Software Engineering, Perth, Australia, 2003.
9. Neumann C, Puch-Solis R, inventors. The Forensic Science Service Ltd., assignee. Improvements in and relating to identifier investigation. U.S. patent application 11/083,822, March 18, 2005, U.K. Patent application 05/02990, February 11, 2005.
10. Neumann C, Puch-Solis R, inventors. The Forensic Science Service Ltd., assignee. Improvements in and relating to identifier comparison. U.S. patent application 11/083,579, May 18 2005, U.K. patent application 05/003961, October 14, 2004.
11. Distribution of NCIC FPC: http://home.att.net/~dermatoglyphics/mfre/
12. Dempster AP, Laird NM, Rubin DB. Maximum-likelihood from incomplete data via the EM algorithm. J R Stat Soc B 1977;39:1–37.
13. Champod C. Reconnaissance automatique et analyse statistique des minuties sur les empreintes digitales. PhD Thesis. Université de Lausanne, Institut de Police Scientifique et de Criminologie, Lausanne, Switzerland, 1996.
14. Stoney DA. Measurement of fingerprint individuality. In: Lee HC, Gaensslen RE, editors. Advances in fingerprint technology. Boca Raton: CRC Press, 2001:327–87.

Additional information and reprint requests:
Cedric Neumann
The Forensic Science Service
2920 Trident Court
Solihull Parkway
Birmingham Business Park
Birmingham B377YN
U.K.
E-mail: cedric.neumann@mac.com